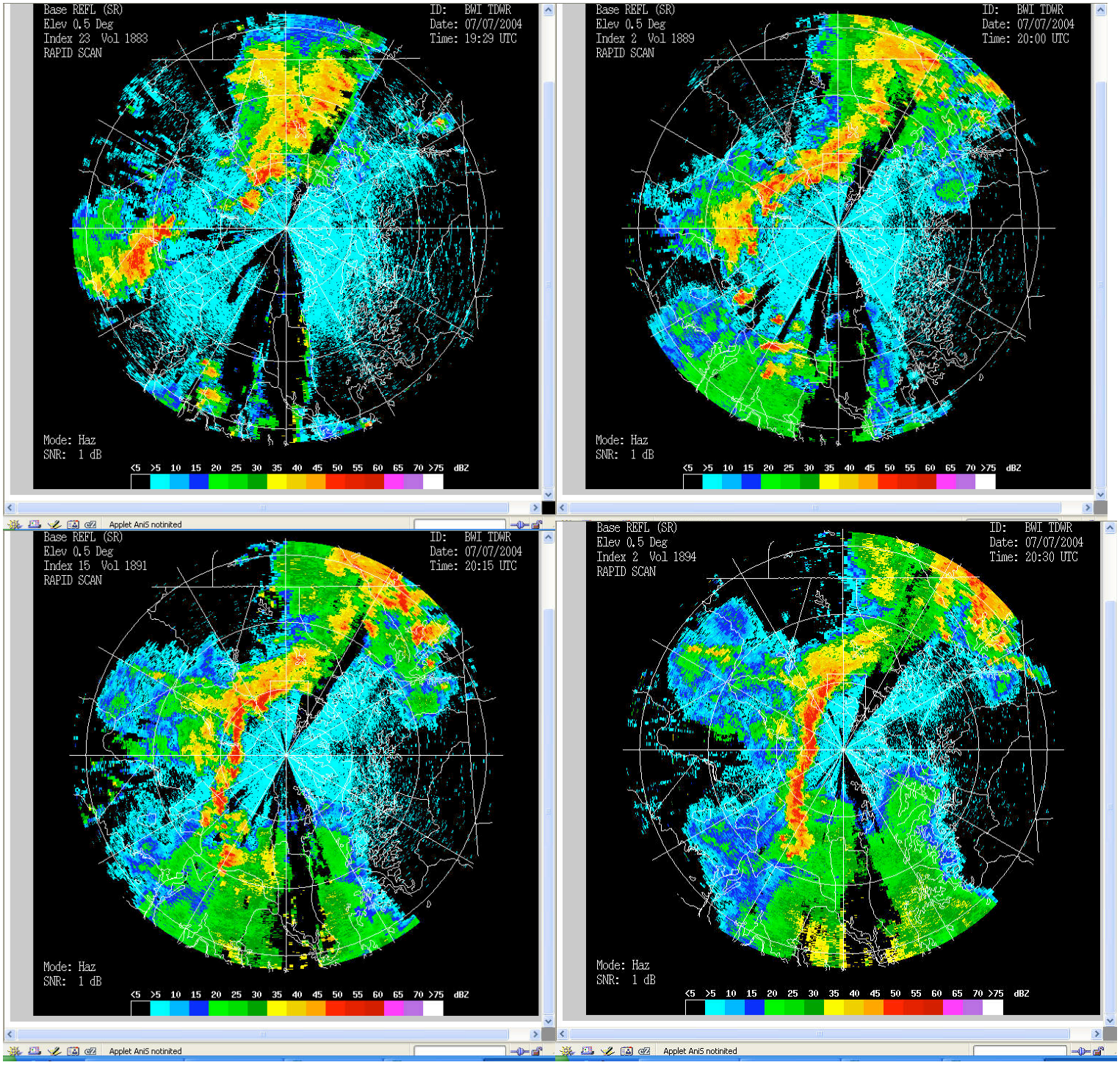

Figure 1. TDWR reflectivity fields for the 0.5 degree elevation angle at 1929, 2000, 2015 and 2030 UTC on 7 July 2004.

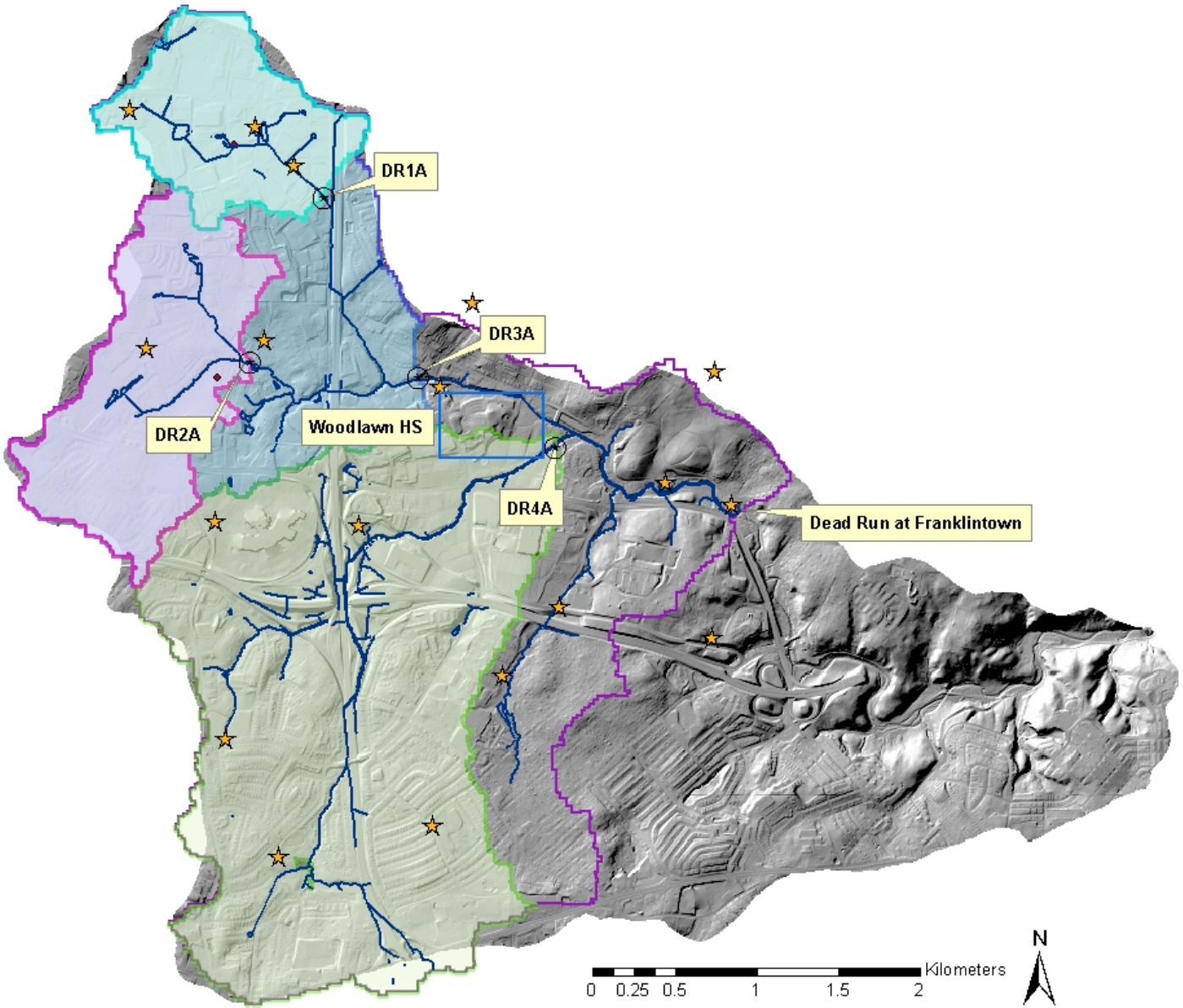

Figure 2. Dead Run drainage basin. The tributary basins DR1 - DR4 are shaded and the outlet of each subbasin is identified. Rain gage locations are indicated by stars.

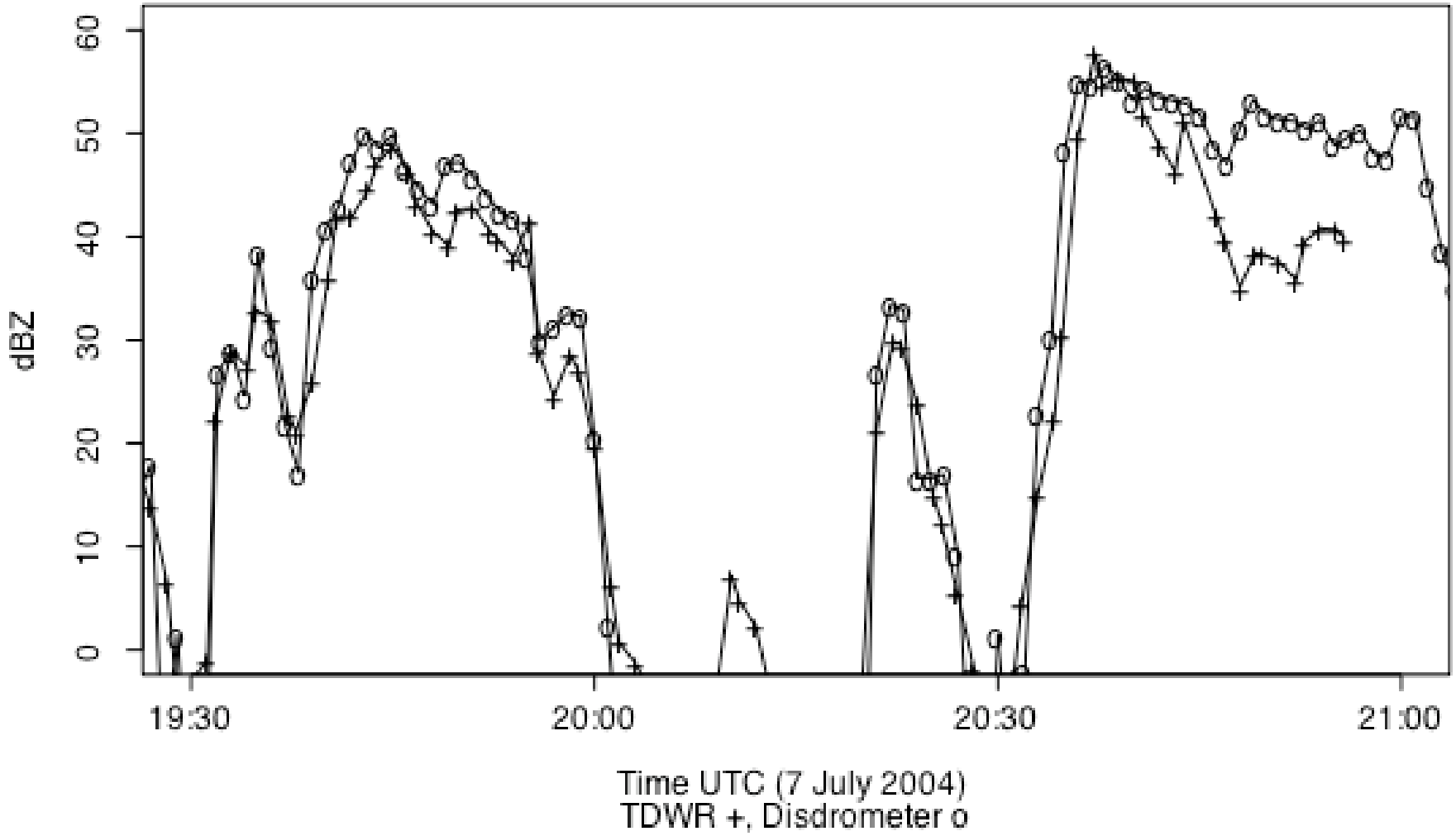

Figure 3. Time series of reflectivity at 1 minute time scale from Joss-Waldvogel disdrometer (at UMBC; “o”) and TDWR (bin containing disdrometer; “+”) on 7 July 2004 (see also Figure 1).

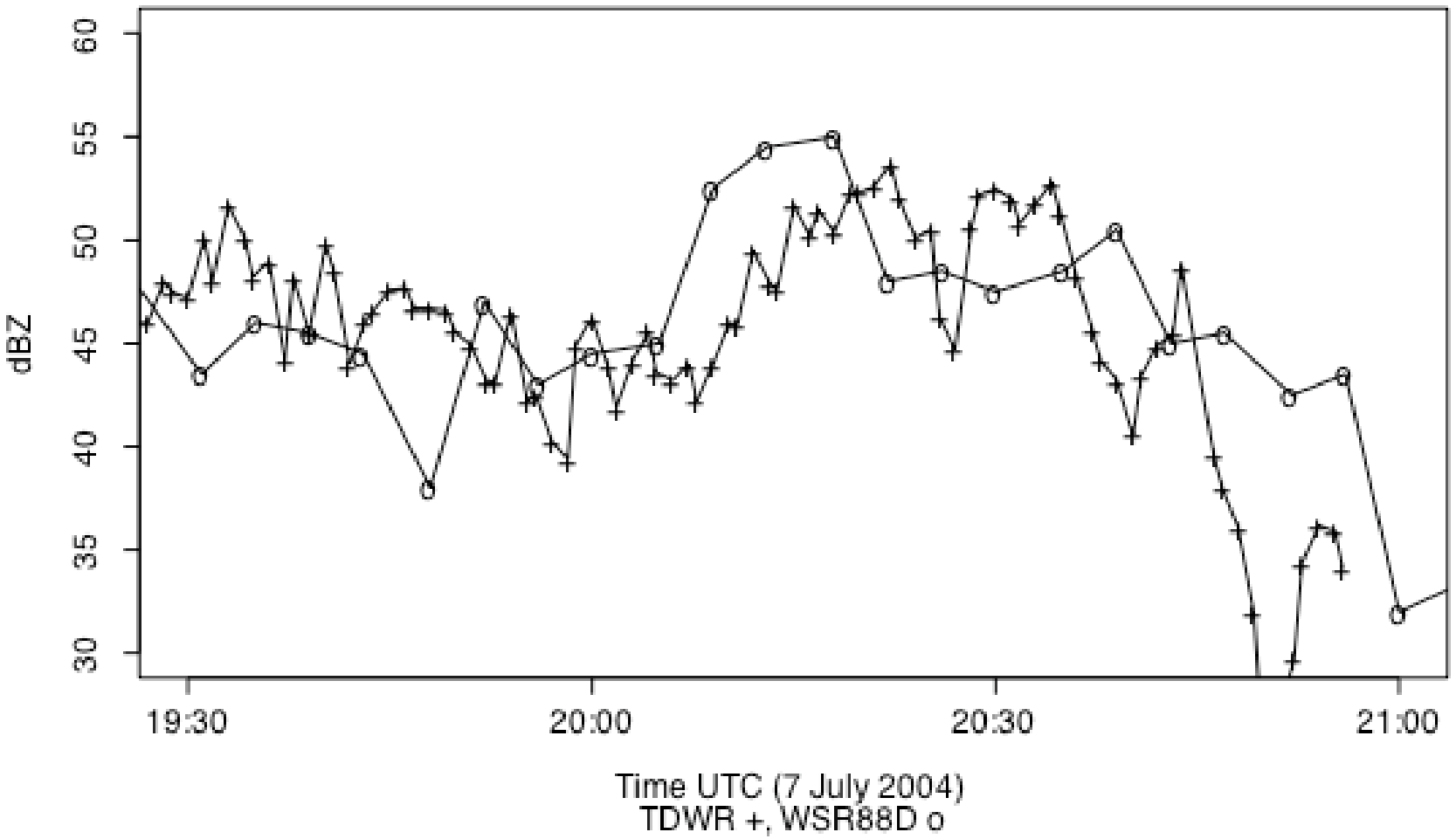

Figure 4. Reflectivity time series from the TDWR and KLWX WSR-88D for the Woodlawn High School rain gage location (that is, the bin containing the rain gage) on 7 July 2004.

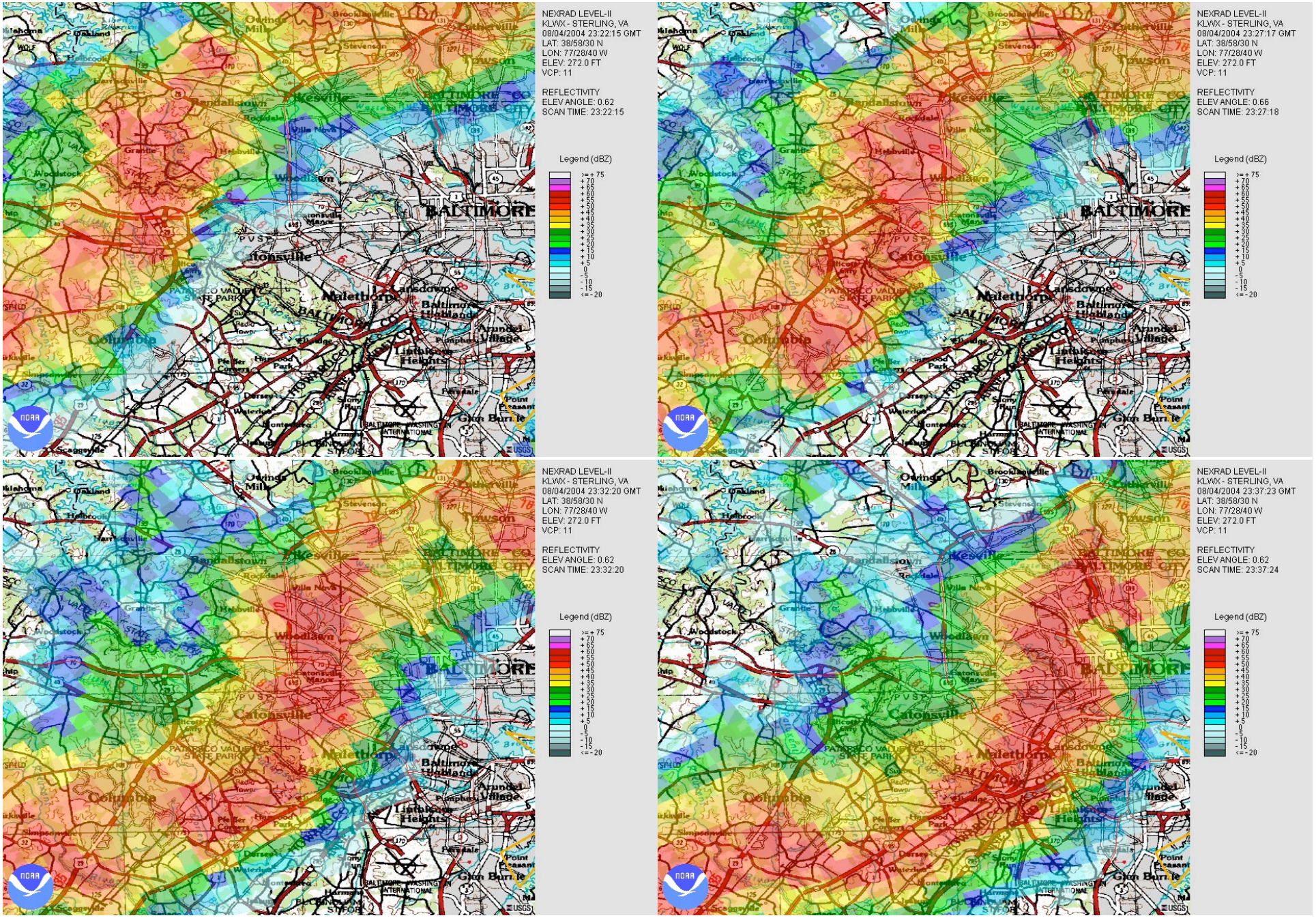

Figure 5. KLWX reflectivity fields at 2322, 2327, 2332 and 2337 on 4 August 2004.

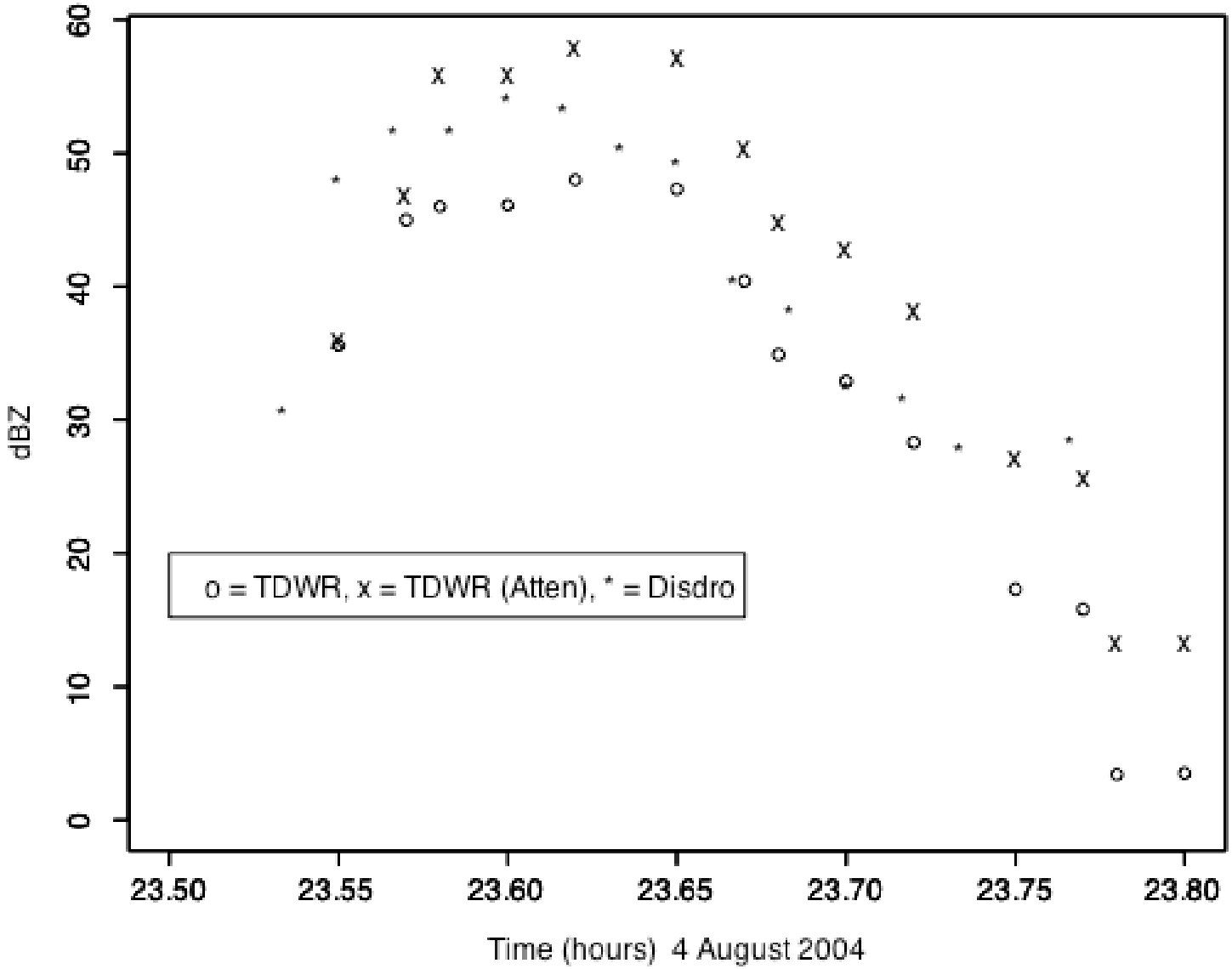

Figure 6. Time series of reflectivity from J-W disdrometer ("*"), TDWR and TDWR with attenuation correction (algorithm 1) on 4 August 2004.

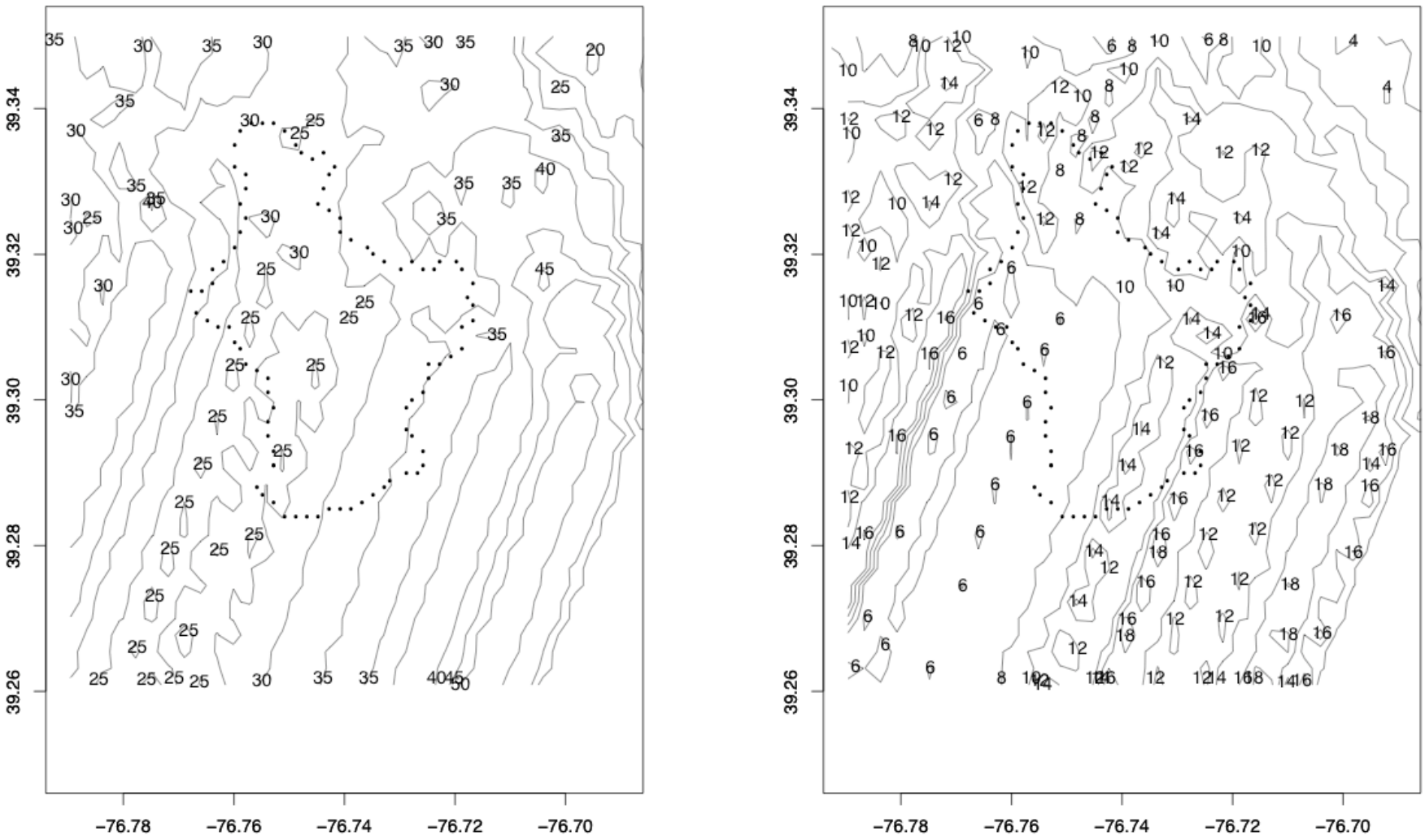

Figure 7. Storm total rainfall estimates (mm) from the TDWR using attenuation algorithm 1 (left) and without attenuation correction (right) for the 4 August 2004 storm. The Dead Run basin boundary (see Fig.2) is denoted by closed dots (see Fig. 2).

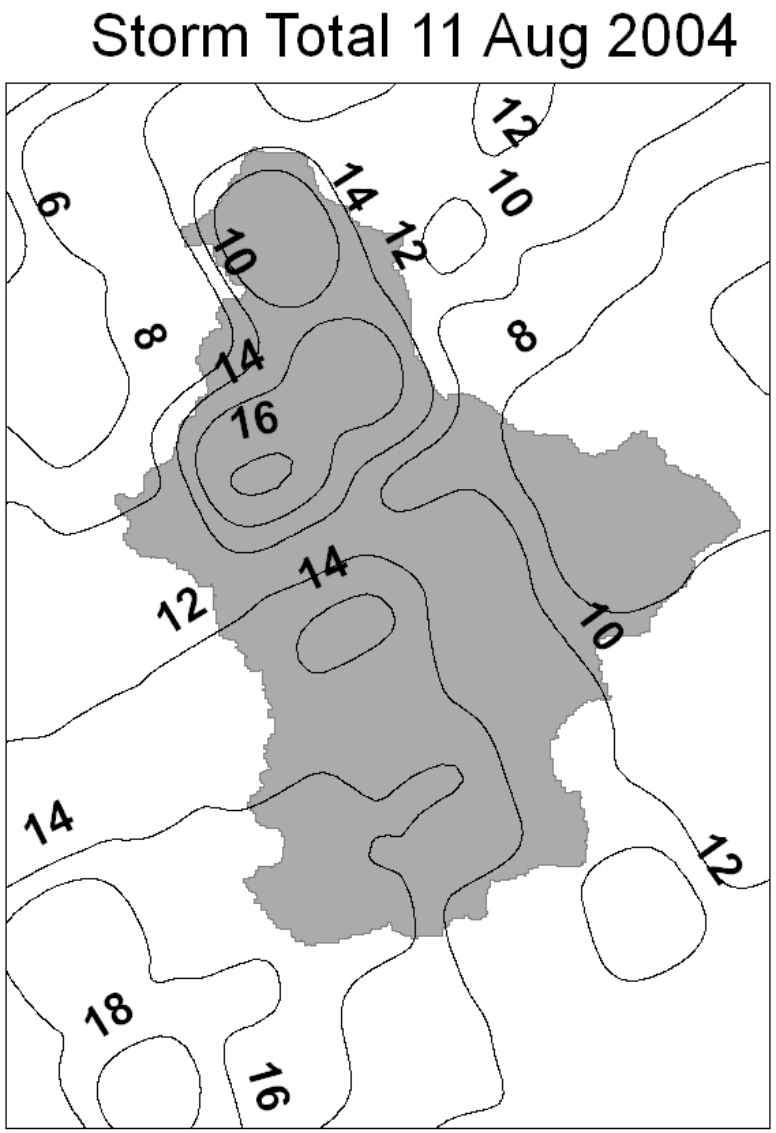

Figure 8. Storm total rainfall estimates (mm) from the KLWX WSR-88D for the 4 August 2004 storm. The Dead Run basin (see Fig.2) is shaded gray.

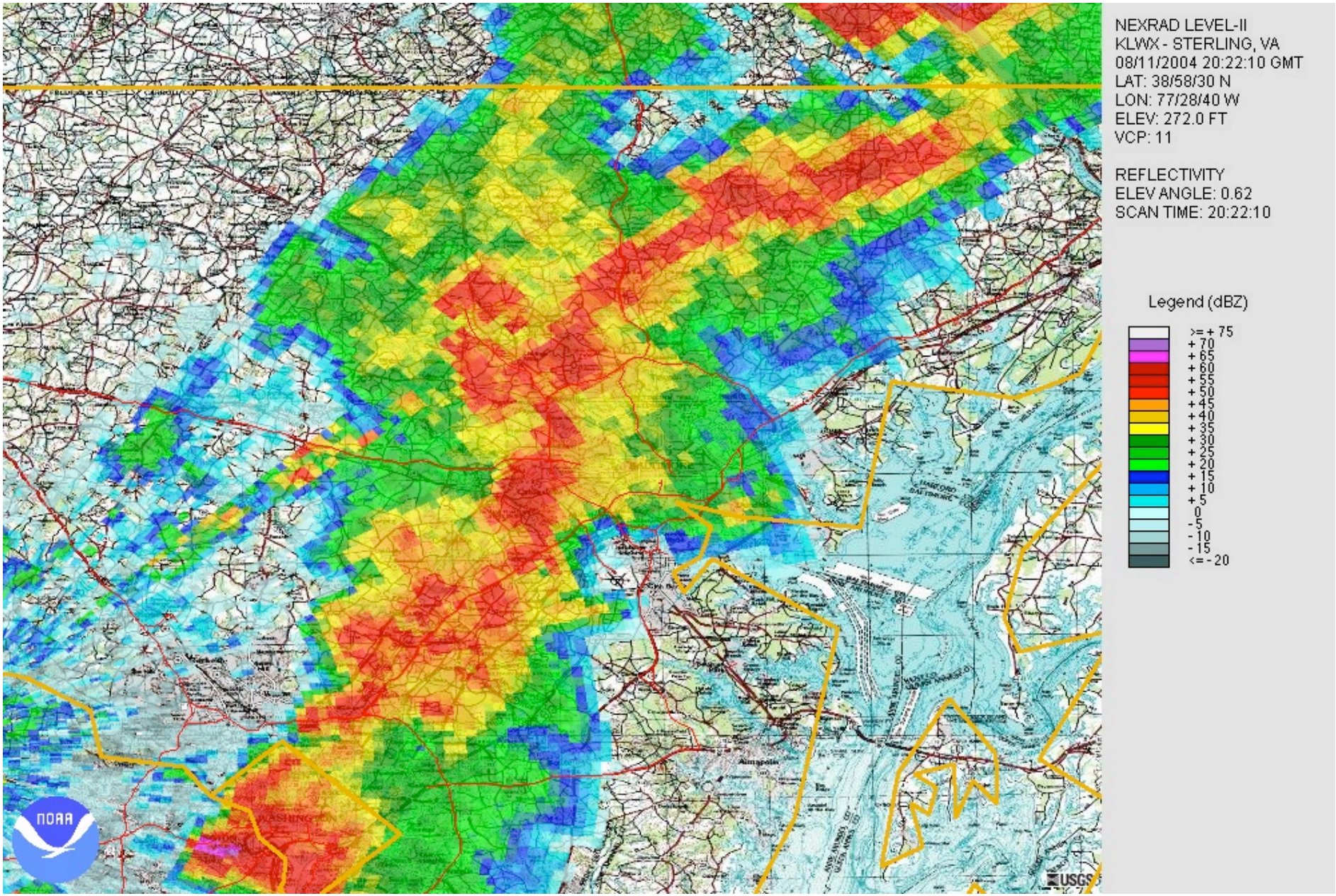

Figure 9. KLWX reflectivity image at 2022 UTC on 11 August 2004.

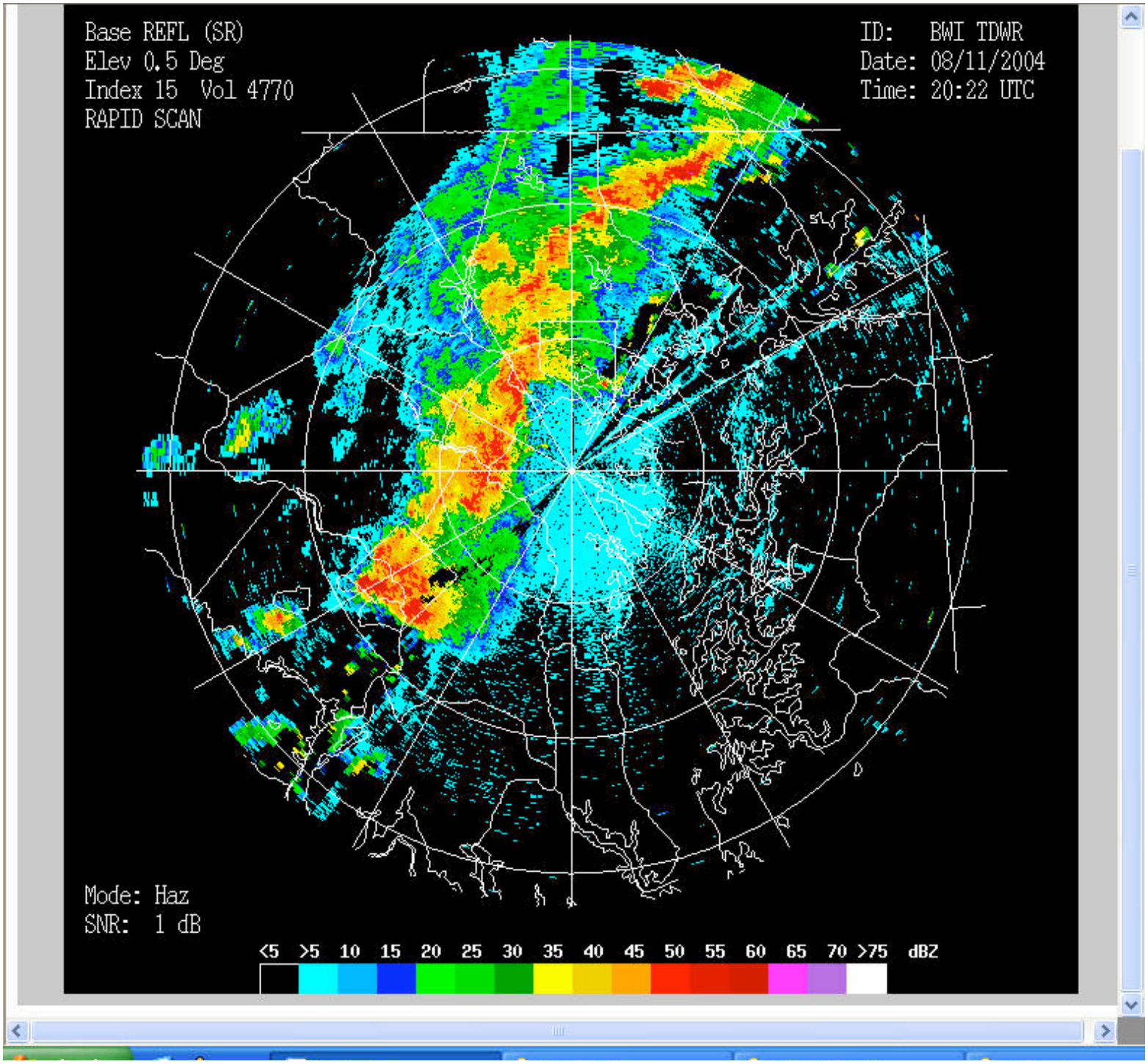

Figure 10. TDWR reflectivity image for the 0.5 degree elevation angle at 2022 UTC on 11 August 2004.

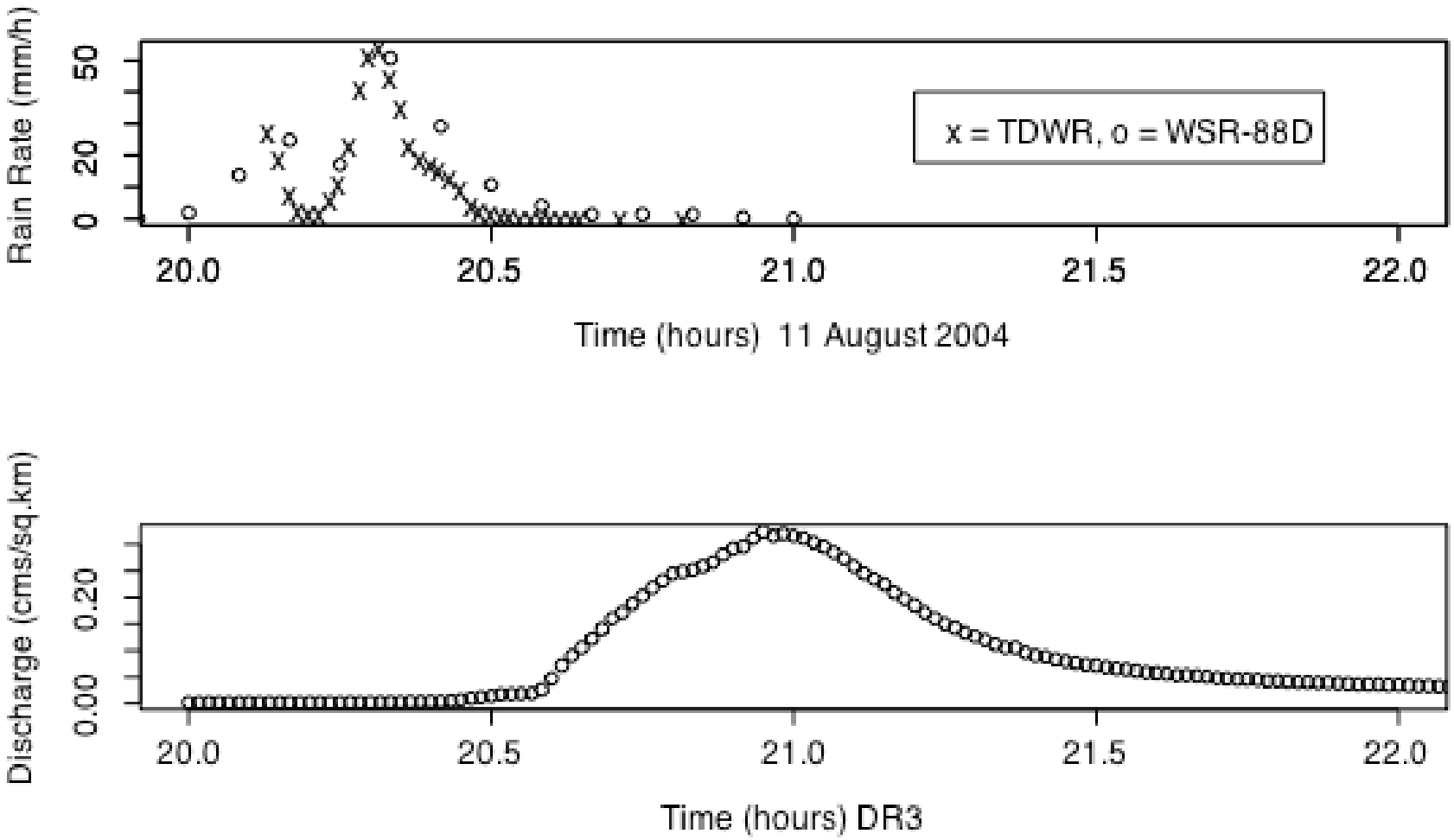

Figure 11. Basin-averaged rainfall rate from TDWR (“x”) and WSR-88D (“0”) for the DR3 subbasin of Dead Run (top) and DR3 discharge time series (bottom) on 11 August 2004.

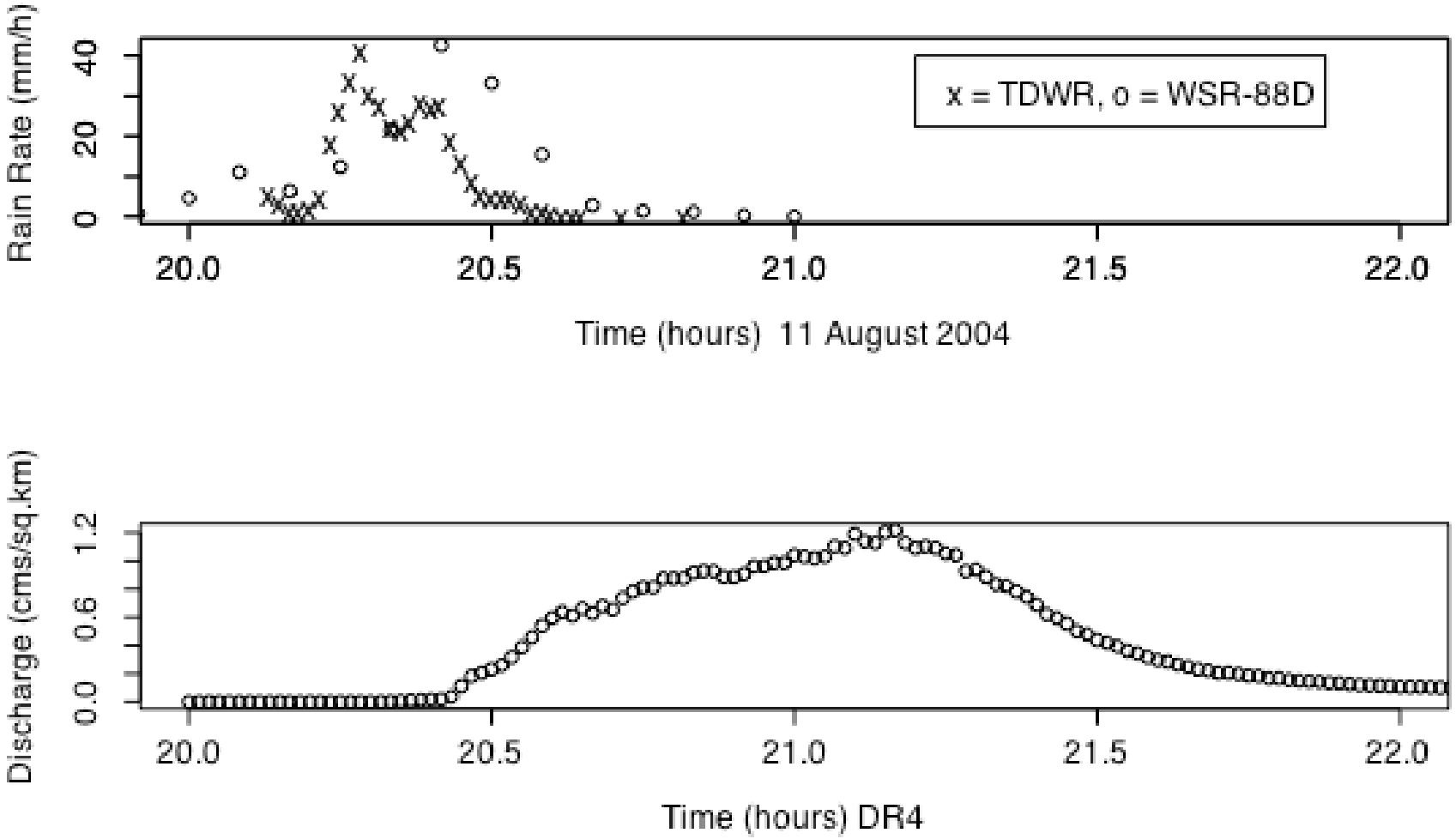

Figure 12. Basin-averaged rainfall rate from TDWR (“x”) and WSR-88D (“0”) for the DR4 subbasin of Dead Run (top) and DR4 discharge time series (bottom) on 11 August 2004.

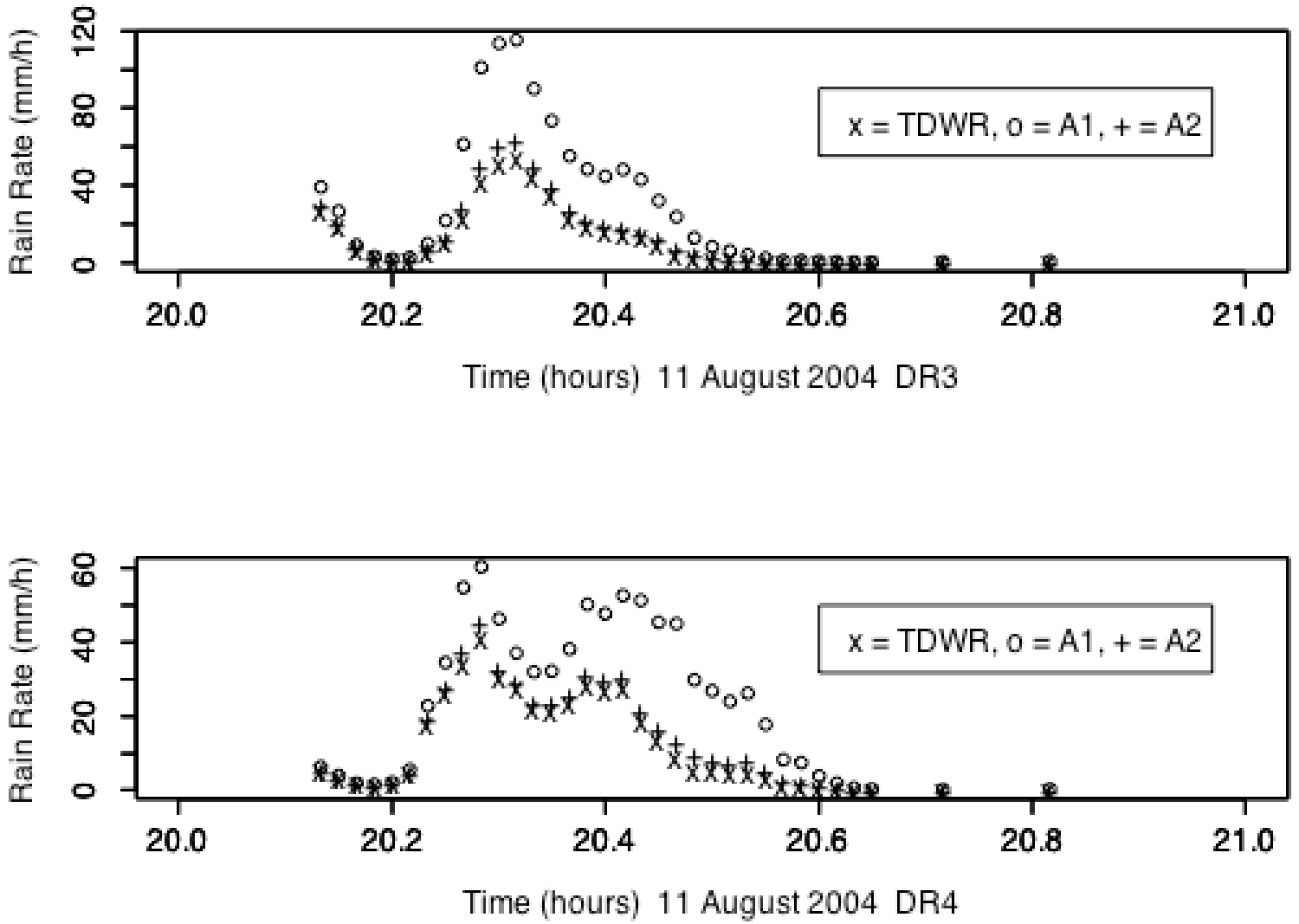

Figure 13. Basin-averaged rainfall rate from TDWR for DR3 (top) and DR4 (bottom) on 11 August 2003. In each figure, results are presented for TDWR rainfall estimates without attenuation correction and rainfall estimates using algorithms 1 (“o”) and 2 (“+”) for attenuation correction.

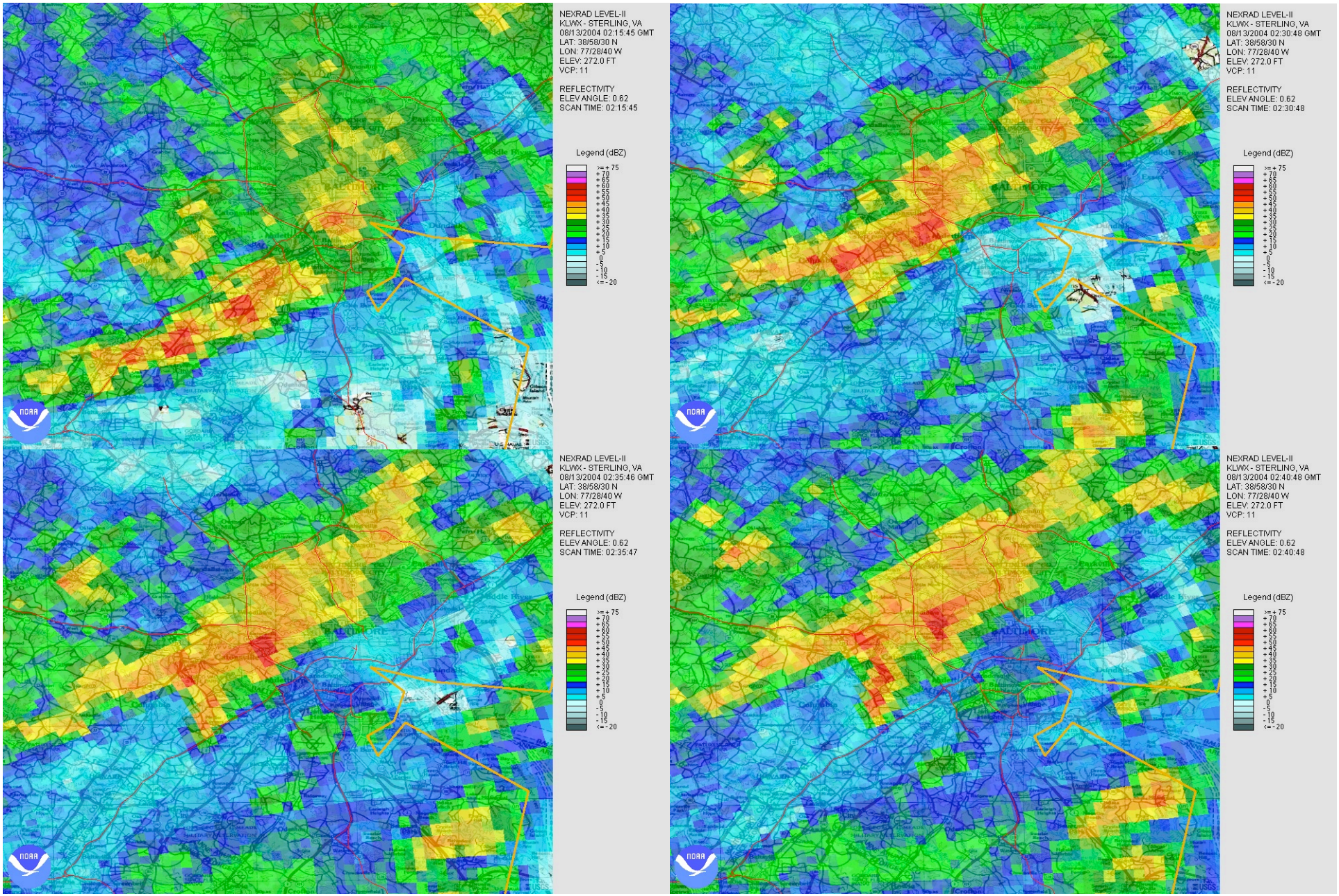

Figure 14. KLWX reflectivity images at 0215 (upper left), 0230 (upper right), 0235 (lower left) and 0240 (lower right) on 13 August 2004.

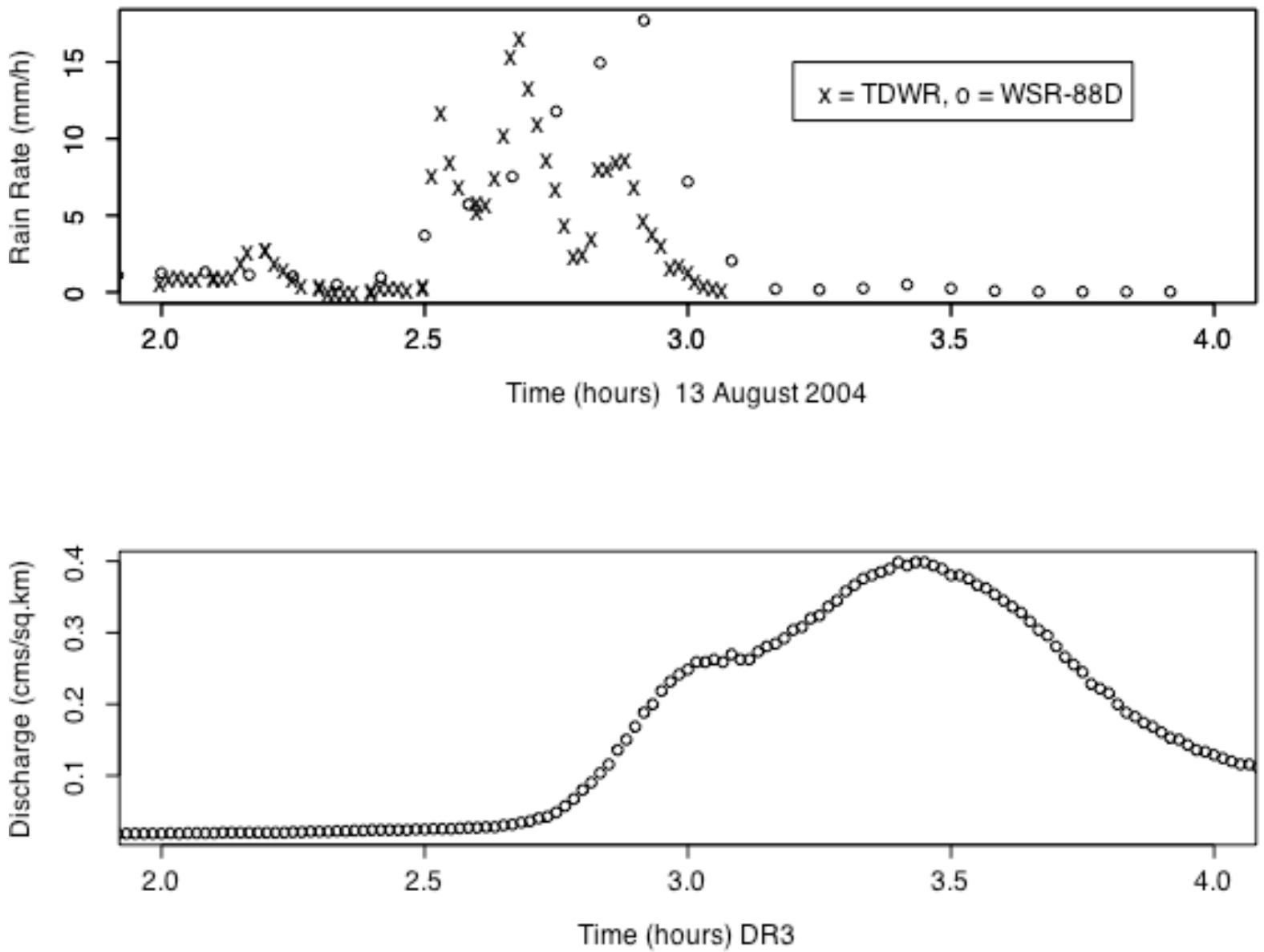

Figure 15. Basin-averaged rainfall rate from TDWR (“x”) and WSR-88D (“0”) for the DR3 subbasin of Dead Run (top) and DR3 discharge time series (bottom) on 13 August 2004.

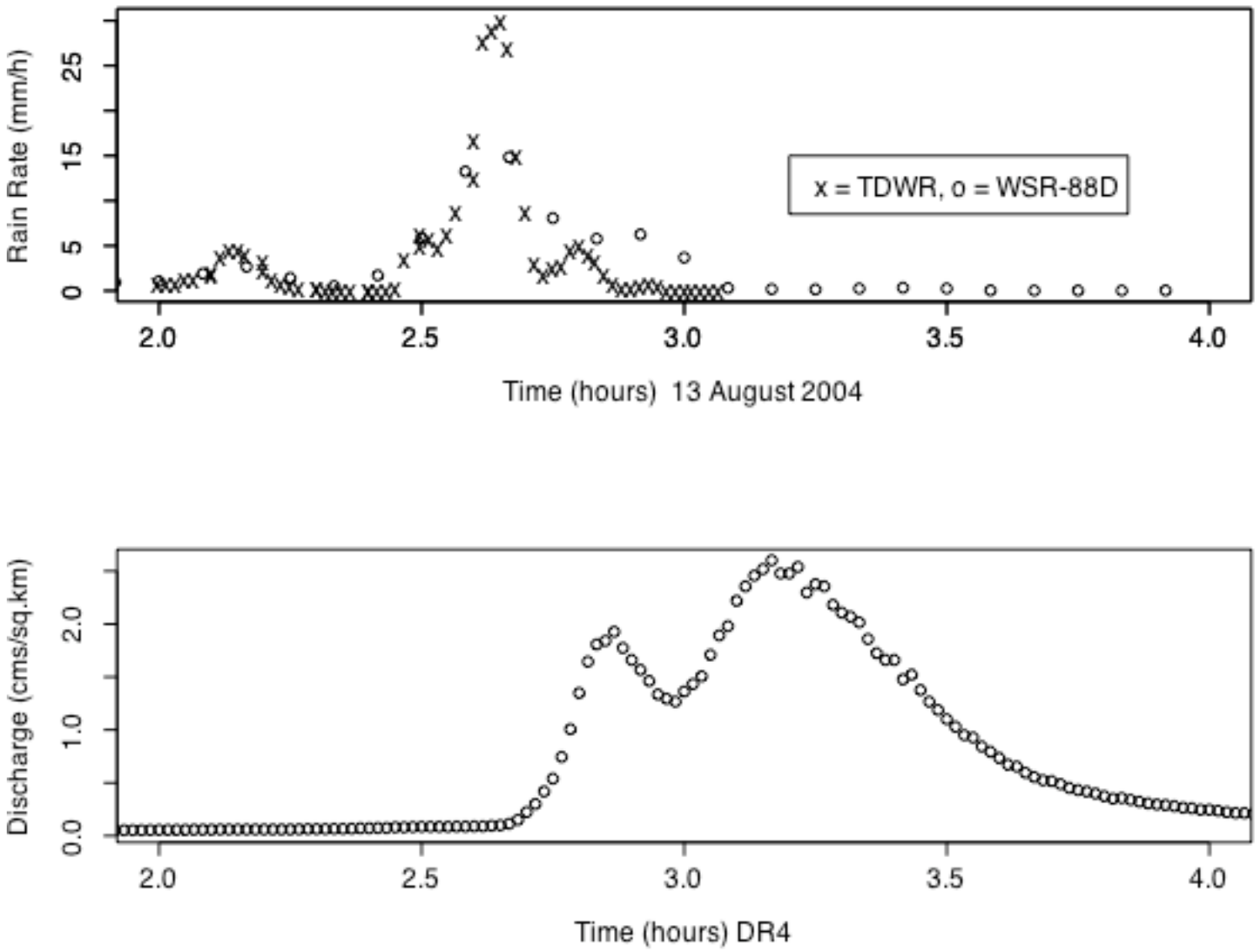

Figure 16. Basin-averaged rainfall rate from TDWR (“x”) and WSR-88D (“0”) for the DR4 subbasin of Dead Run (top) and DR4 discharge time series (bottom) on 13 August 2004.

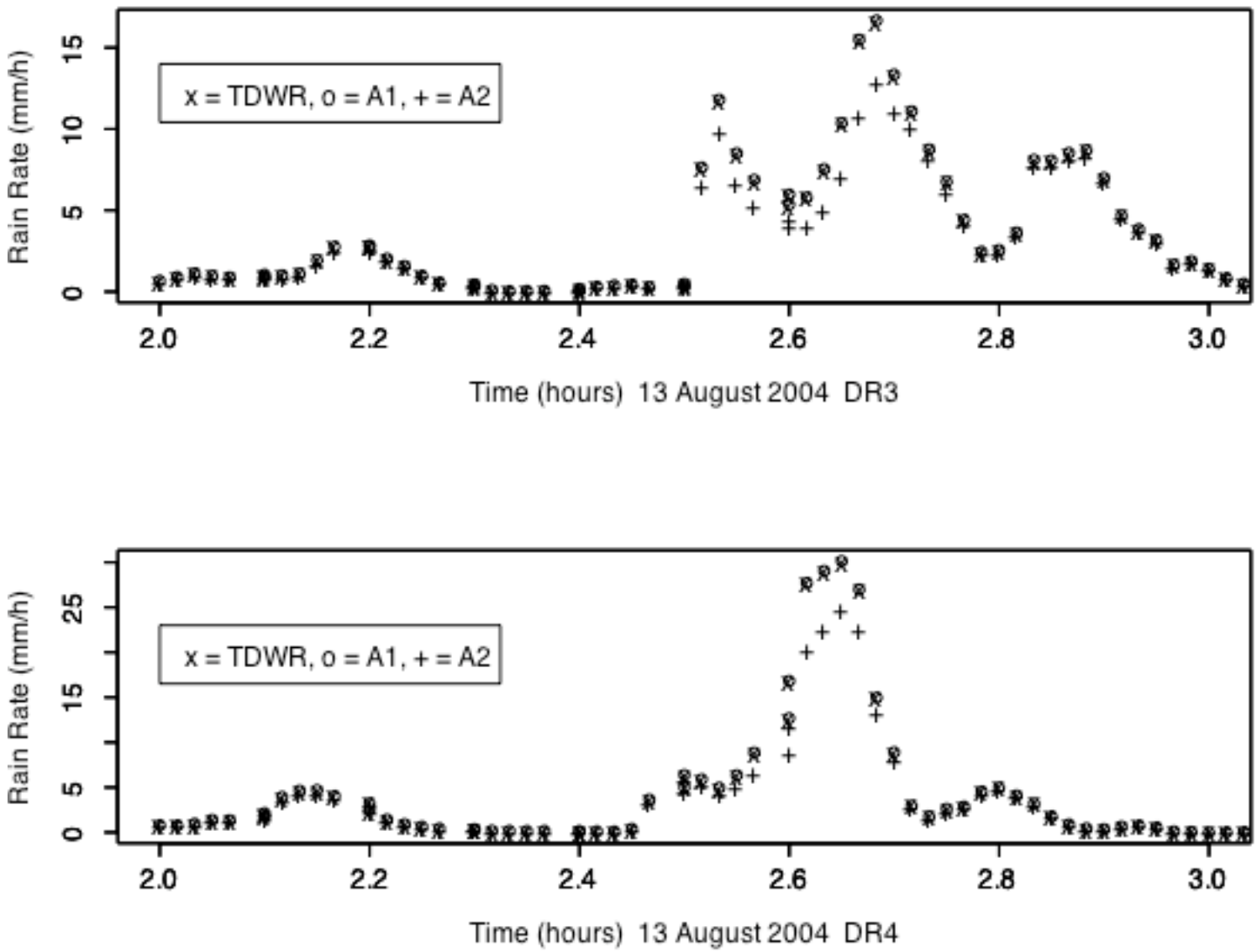

Figure 17. Basin-averaged rainfall rate from TDWR for DR3 (top) and DR4 (bottom) on 13 August 2003. In each figure, results are presented for TDWR rainfall estimates without attenuation correction and rainfall estimates using algorithms 1 (“o”) and 2 (“+”) for attenuation correction.

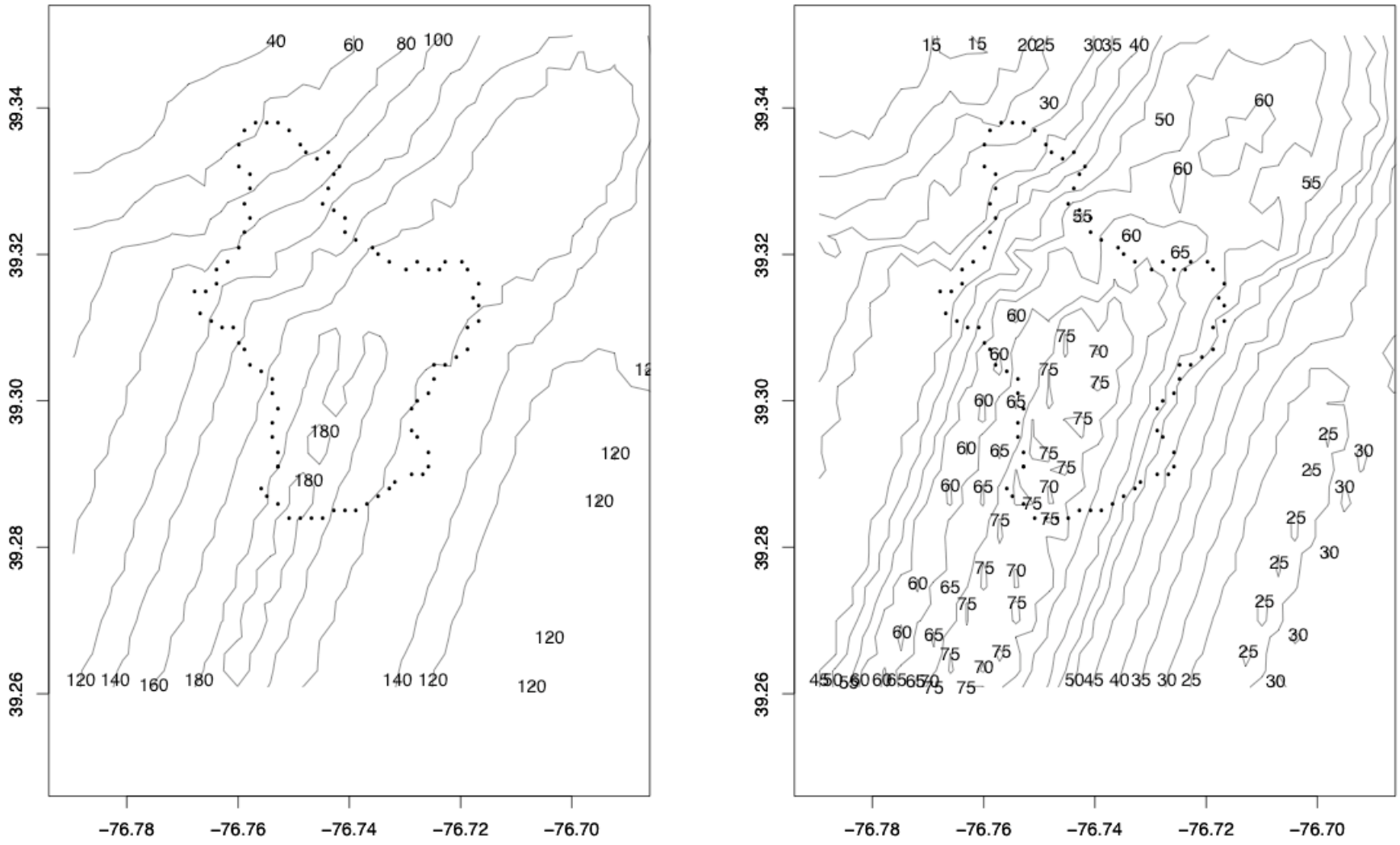

Figure 18. Storm total rainfall estimates (mm) from the TDWR using attenuation algorithm 1 (left) and without attenuation correction (right) for the 7 July 2004 storm. The Dead Run basin boundary (see Fig.2) is denoted by closed dots

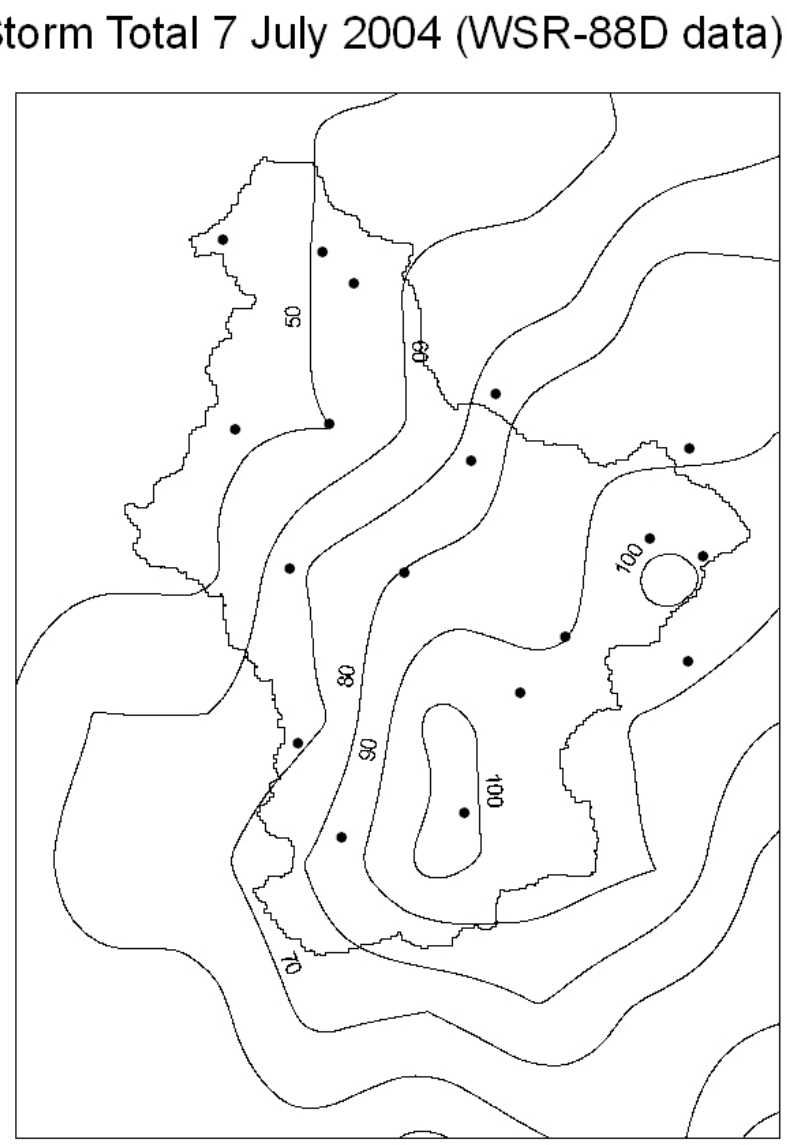

Figure 19. Storm total rainfall estimates (mm) from the KLWX WSR-88D for the 7 July 2004 storm. The Dead Run basin boundary (see Fig.2) is outlined.

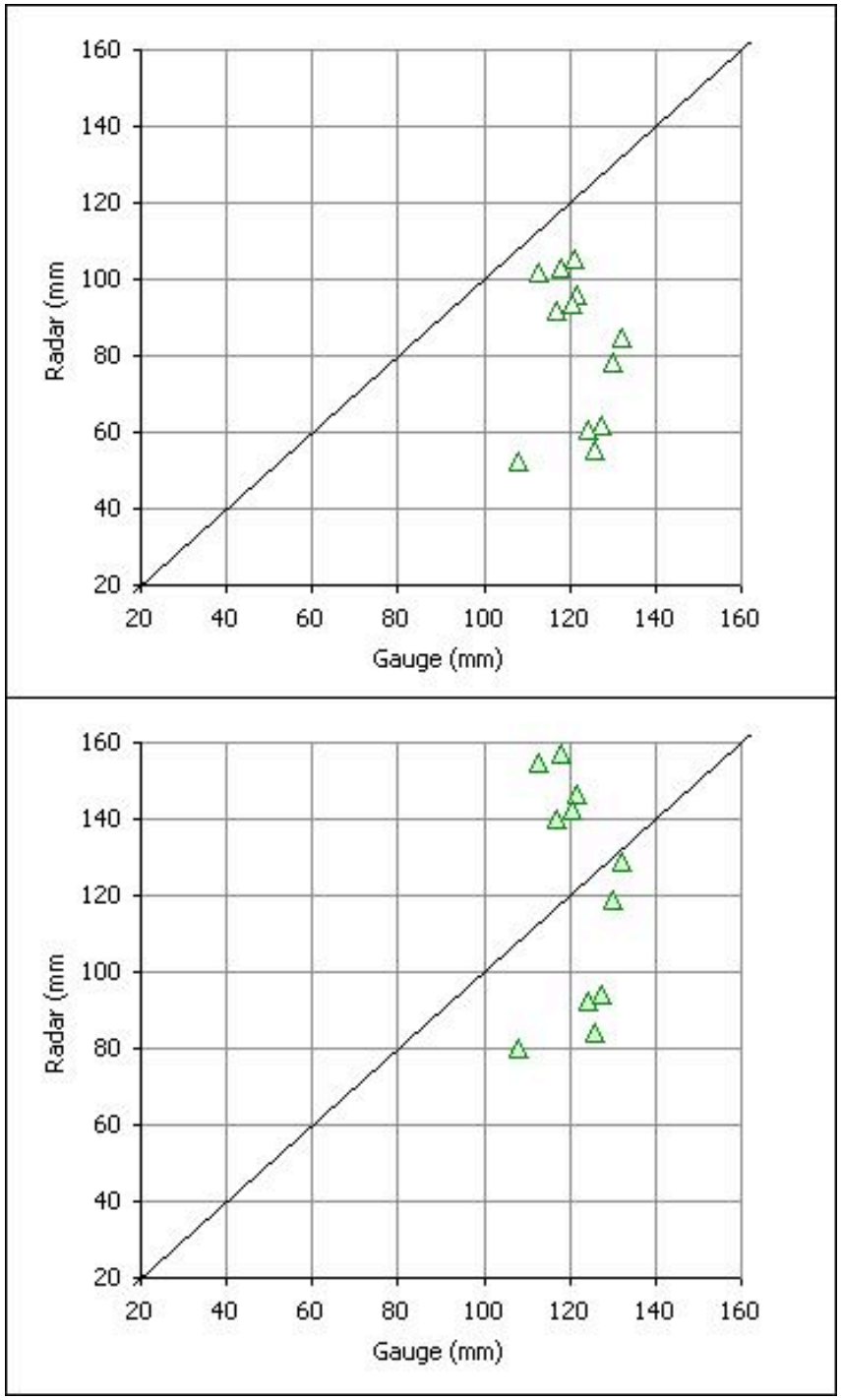

Figure 20. Gage - radar intercomparsions for WSR-88D storm total rainfall estimates for 7 July 2004. The bottom graph is for storm total WSR-88D rainfall estimates with bias correction. The top graph is based solely on the convective Z-R relationship and does not include bias correction.

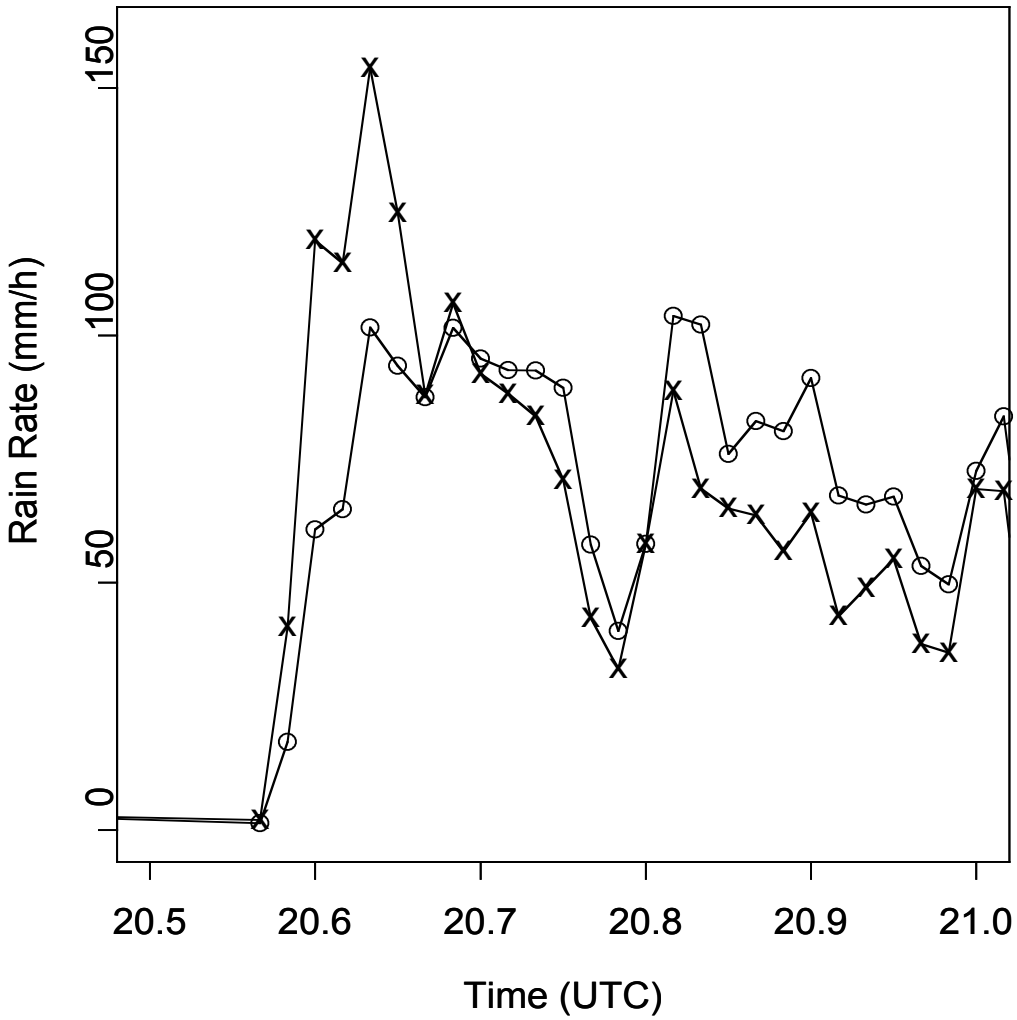

Figure 21. Intercomparsion of rainfall rate computed directly from disdrometer drop spectra measurements (open circles) and from rain rate computed by applying the convective Z-R relationship to disdrometer measured Z for the 7 July 2004 storm.

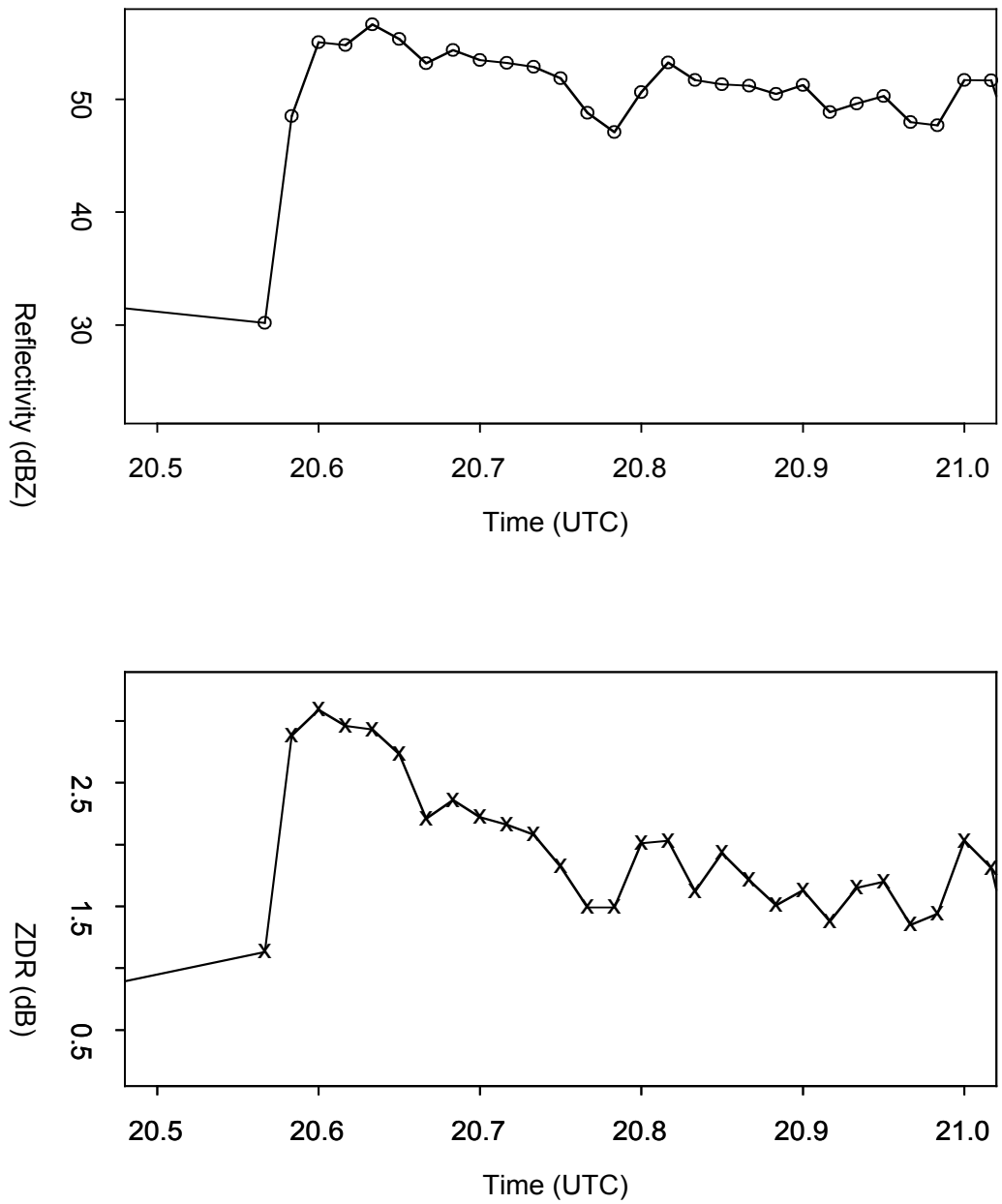

Figure 22. Disdrometer time series of Z and Z_{DR} for the 7 July 2004 storm.

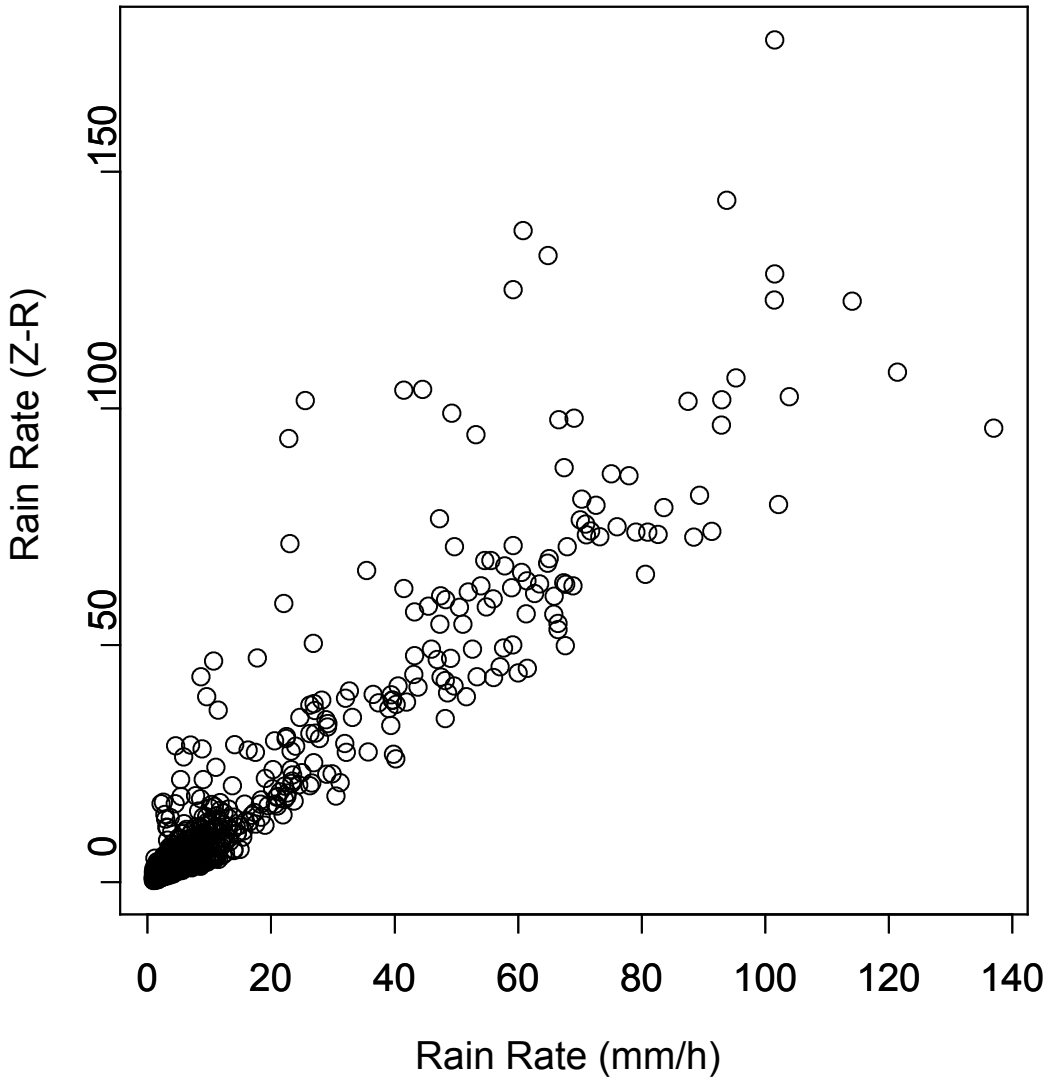

Figure 23. Intercomparison of disdrometer rain rates and rain rates computed from the convective Z-R relationship using disdrometer reflectivity for the 7 July 2004 storm.

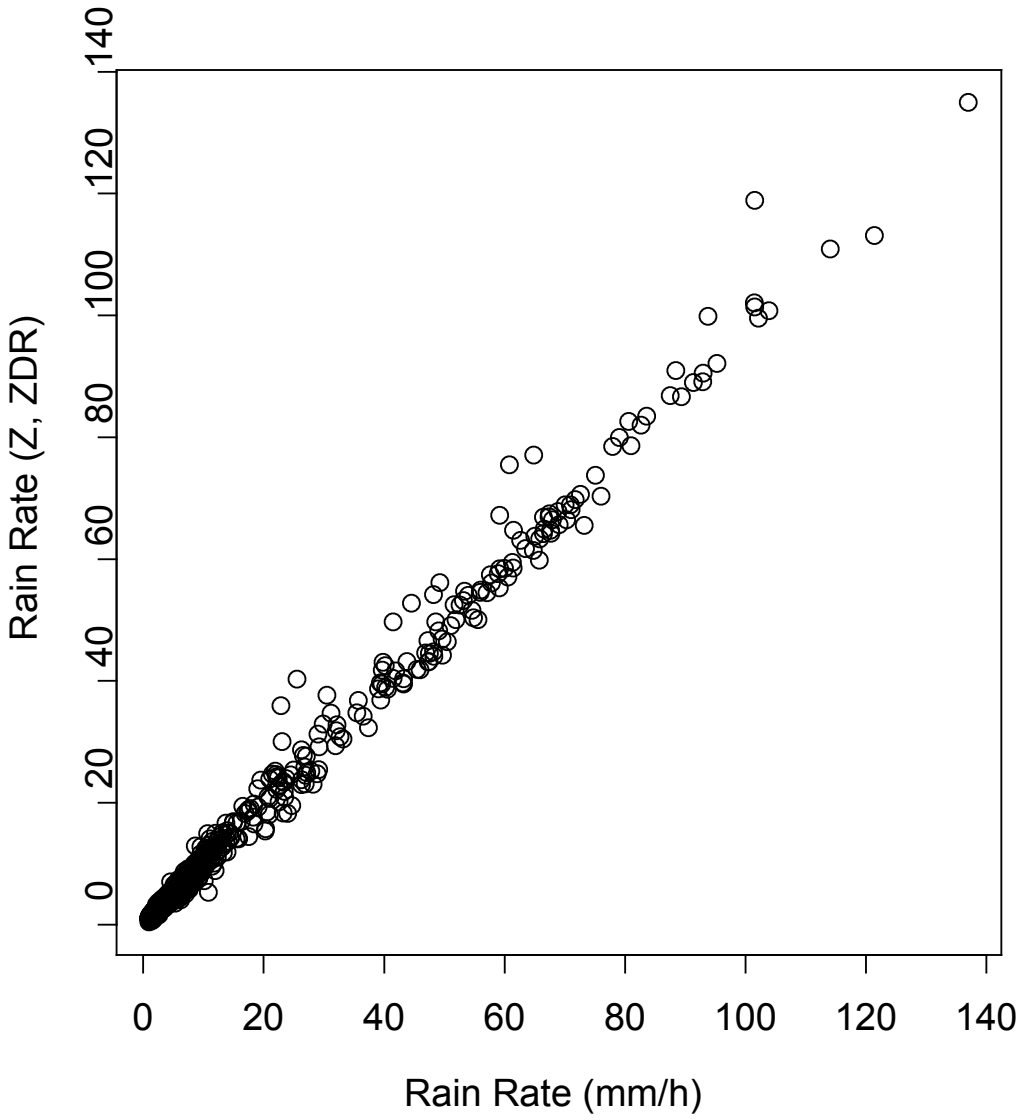

Figure 24. Intercomparison of disdrometer rain rates and rain rates computed from a modified (Z, ZDR) algorithm using disdrometer Z and ZDR for the 7 July 2004 storm.